Supplementary Figures

Figure S1. Predicted responses of two-kinesin velocities and microtubule bound configurations in the force clamp when force feedback algorithms are activates at different applied loads. All plots were generated using the mechanical modeling procedures and the transition rate model described in the Supporting Methods and references S1 and S2. (**A**) Model predictions of the time dependence of bead velocities when they are transported by two-kinesins in the force clamp against a constant applied load of 5 pN. Dependencies for cases where beads were first allowed to be transported to loads of 3 pN (*red*), 7 pN (*blue*) and 8 pN (*black*) prior to the activation of the force clamp are shown. (**B**) Predictions of the force dependence of the probability a two-kinesin complex will bind the microtubule in a configuration supporting load-sharing between its motors at the time the force clamp is first activated (*blue*), and after the system has reached a steady-state (*black*). Kinesins within a complex are assumed to share their load if the trailing motor bears at least 35% of the applied load on the bead. The intersections of the red and blue lines denote the initial probability motors would share their load when F_{Trig} was set to 3, 7 and 8 pN in our model. The intersections of the black lines indicate the load-sharing probability for the motors when the system has reached its steady-state. The arrows indicate the changes in the state distributions that are expected to occur in the experiments in Figures 5 and S1A. (**C** - **E**) Plots showing the evolution of a complex's distribution of 2-motor bound configurations in the force clamp. A complex's bound state is specified by the separation distances between its microtubule-bound motors. Plots are shown for cases where F_{trig} was set to 3 pN (**C**), 7 pN (**D**) and 8 pN (**E**). According to our mechanical model, configurations where the trailing motor assumes 35 – 50 % of the applied load in these plots correspond to separation distances ranging between 0 - 4 steps (0 - 40 nm). Note, the peaks at $t = 0$ in D and E are broader than the corresponding peak at steady-state ($t \geq 1$ s) in each plot.

Figure S2. Calculated two-kinesin velocities in the force clamp over a range of applied loads. The blue and black lines correspond to the calculations where the force clamp was triggered at 2 and 9 pN respectively. Note, the probability a motor complex will exhibit load-sharing behaviors reaches a saturation point when the force clamp is initiated at $F_{trig} \geq 9$ pN (Figure S1B). For both cases, initial and average bead velocities are indicated by the large dashed and solid lines respectively. The grey dashed line in-between the blue and black plots indicates the steady-state velocities in the force clamp. The inset shows the normalized difference in two-kinesin velocities, $[\langle v(F_{ap};\ F_{Trig} = 9\text{ pN})\rangle - \langle v(F_{ap};\ F_{Trig} = 2\text{ pN})\rangle] / \langle v(F_{ap};\ F_{Trig} = 2\text{ pN})\rangle$, and indicates these extent to which average velocities deviate between the solid curves.

Figure S3. Two-kinesin velocities are predicted to deviate in static trapping and force clamp assays above kinesin's stalling force. Bead velocities in the static trap and force clamp deviate very little below kinesin's stalling force. However, the bead velocities increase non-monotonically with increasing load in the static trap and are higher than those predicted for the force clamp assays when the load exceeds 7 pN. As discussed in the text, this behavior stems from the fact that applied loads decrease in the static trap when beads detach partially from their filament but remain constant in the

force clamp. Thus, the number of single-motor-bound states that contribute to bead velocities at high loads is lower in the static trap than in the force clamp. The dashed curve denotes the *F*-*V* relationship for two kinesins assuming the motors share their load equally. Note, our model does not account for interactions between the motors that would allow them to function synergistically and produce the high velocity we find in our optical trapping experiments. Furthermore, tests of the model with three motors have not produced these high-velocity behaviors either (*see supporting information in reference S2*).

Fig. S1

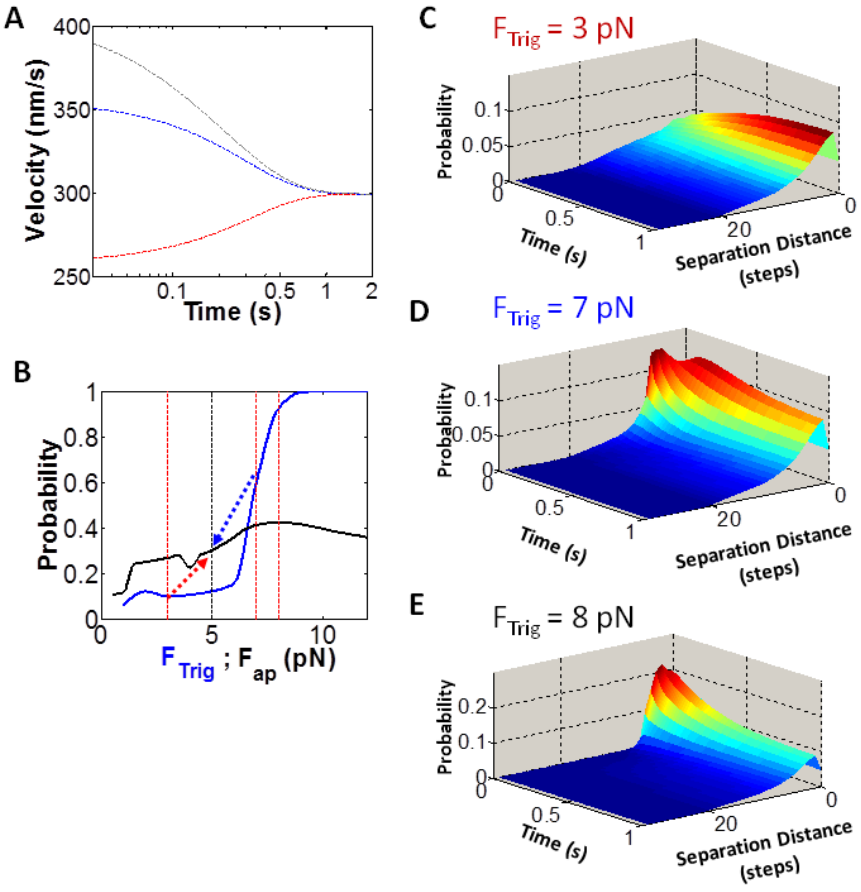
A
Velocity (nm/s)
400
350
300
250
0.1
0.5
1
2
Time (s)
B
Probability
1
0.8
0.6
0.4
0.2
0
0
5
10
F Trig ; F ap (pN)
C
F Trig = 3 pN
Probability
0.1
0.05
0
0
0.5
1
Time (s)
0
20
Separation Distance (steps)
D
F Trig = 7 pN
Probability
0.1
0.05
0
0
0.5
1
Time (s)
0
20
Separation Distance (steps)
E
F Trig = 8 pN
Probability
0.2
0.1
0
0
0.5
1
Time (s)
0
20
Separation Distance (steps)

Fig. S2

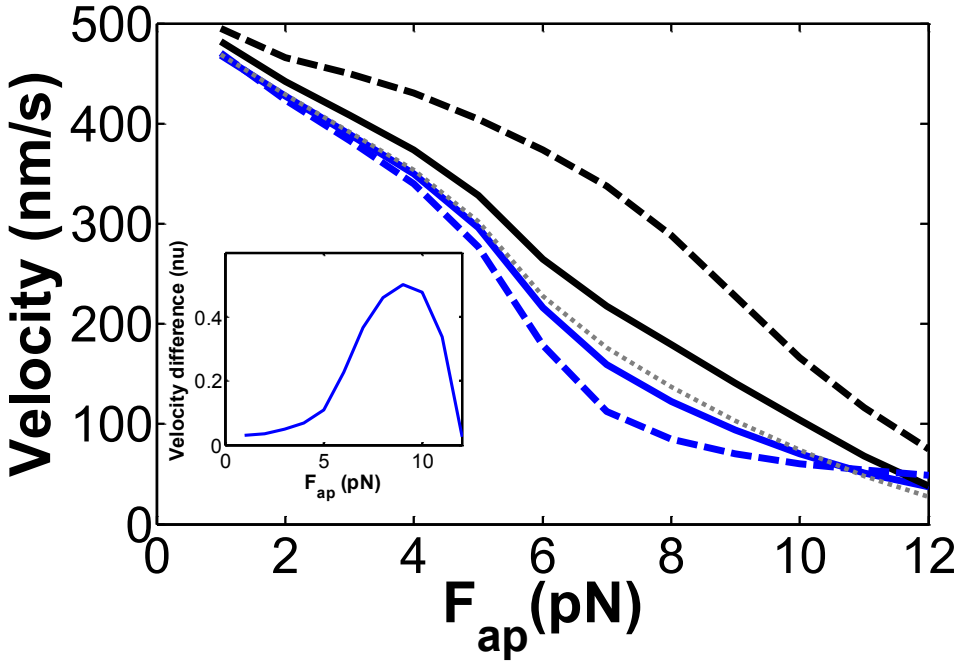
Velocity (nm/s)
500
400
300
200
100
0
0
2
4
6
8
10
12
F ap (pN)
Velocity difference (nu)
0.4
0.2
0
0
5
10
F ap (pN)

Fig. S3

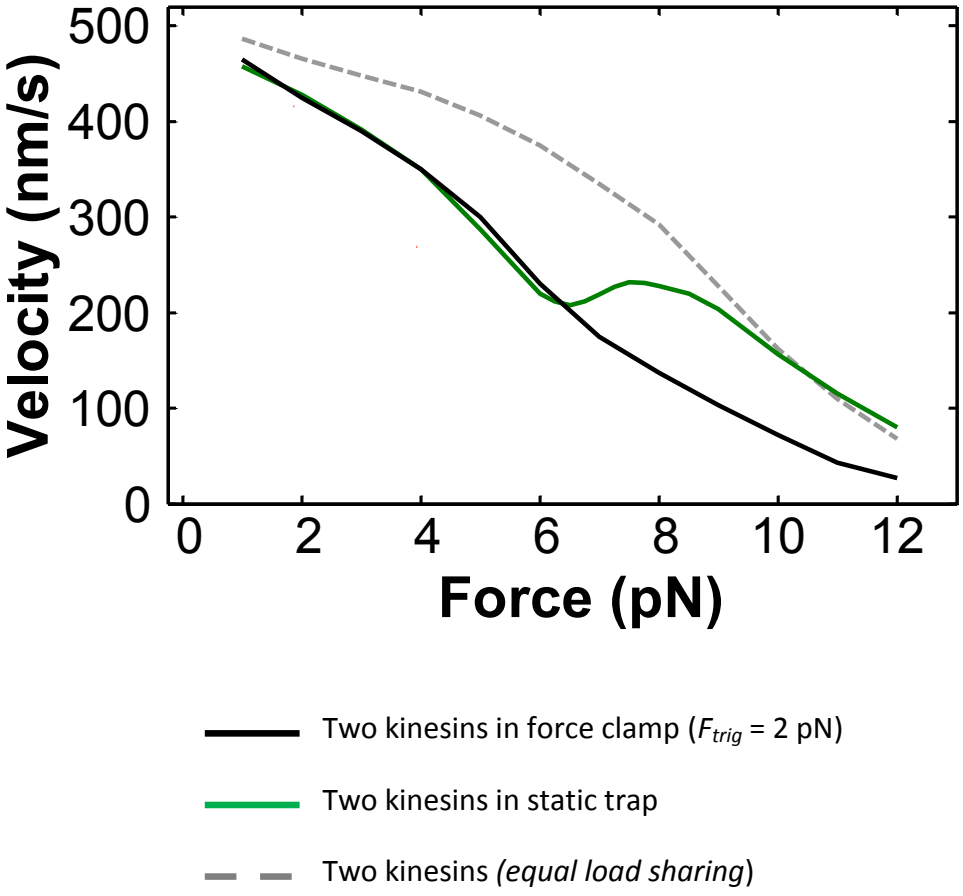
Velocity (nm/s)
500
400
300
200
100
0
0
2
4
6
8
10
12
Force (pN)
Two kinesins in force clamp (F_{trig} = 2 pN)
Two kinesins in static trap
Two kinesins *(equal load sharing)*

Supplementary Methods:

Optical trapping

As in single-kinesin force-clamp assays (S3), a 1064 nm trapping laser (Spectra Physics, Santa Clara, CA) is first used to position a bead over the microtubule. The kinesins can then bind to the filament and transport the bead along the microtubule against the increasing load of the trap. Once the applied load on the bead reaches a specified force threshold (F_{Trig}), acousto-optic deflectors (IntraAction Corp, Bellwood, IL) are used to change the applied load on the bead by moving the trapping beam in the sample plane. A feedback algorithm is used to update the trap laser position at 200 Hz in order to maintain a constant distance between the bead and trap center positions, and hence, a constant load on the bead as it is transported along the microtubule. Bead positions are detected by measuring the deflections of a second 830 nm laser (Point Source, Rochester, NY) in the back-focal plane of the instrument's condenser objective. The detection laser position remains fixed throughout the assay. In the event a bead is transported towards the edge of the calibrated region of the detection system, a nano-positioning stage is used to displace the bead back towards the center position of the detection laser. The feedback algorithm of the force clamp remains activated during this process.

Mechanical modeling and analyses of multiple kinesin transition rates

Configuration-dependent load distributions within the two-kinesin complexes were analyzed using the mechanical modeling procedure described in reference S1. In this procedure, we specify positions of the motors on the bead and on the microtubule, as well as the position of the trap and the position and orientation of the bead for each bound configuration of a complex we consider in our model. Our optical trapping calibration procedures and measurements of single kinesins stiffnesses are used to specify the spring constants for the trap and each kinesin-bead linkage in the complex. With this information, a complex's 'equilibrium' configuration can be found via an energy minimization where the bead moved until a position is found where the forces on the motors and the bead, as well as the torque on the bead, are balance within 0.01 fN. Afterwards, the mechanical energy of this geometry, which we call "configurational energy", is calculated by taking the sum of the stretching energies of the trap (*a linear spring*) and the motors (*nonlinear springs*):

$$E_{\mathrm{config}} = \tfrac{1}{2}\kappa_{\mathrm{T}}(x_{\mathrm{T}} - x_b)^2 + \sum_{\mathrm{M}} \int_{l_{\mathrm{o}}}^{l_{\mathrm{ax}}} \left\| \vec{F}_{\mathrm{ax}} \right\| dl,$$

where, κ_T is the trap's spring constant, $x_T - x_b$ is the distance a bead is displaced from the trap center, l_{ax} is the length of a motor when it experience a force (F_{ax}) along its stalk axis, and l_o is the length of an unloaded motor.

Our transition rate model uses the above analyses to predict the rates that motors will exchange between different configurations via motor stepping, binding, and detachment. Each of these rates is assumed to depend on the difference in a complex's configurational energy (ΔE_{config}) before and after a transition. With this treatment, the behavior of two-kinesin complexes in the trap can be analyzed by solving a system of master equations numerically that describe how the complex transitions between each of its available configurations. Importantly, a wide range of configurations (states) are enumerated

in this model, and our approach allows time-dependent probabilities that a complex will adopt different bound configurations to be calculated. All supplementary figures were generated via a numerical calculation that emulates the loading conditions of the static trap and predicts the distributions of a complex's bound configuration when the beads reach a load equally to F_{trig}. A second calculation was then performed to examine how the complex's distribution of bound configurations evolves from this distribution when the applied load is held constant by the force clamp. Motor stepping rates and bead velocities and motor-microtubule binding were calculated using our model as previously described. The details surrounding these calculations are described in reference S2.

S1 Jamison, D. K. , Driver, J. W. , Rogers, A. R. , Constantinou, P. E. , and Diehl, M. R. (2010) *Biophys. J.* **99**, 2967-2977.

S2 Driver, J. W. *et al.* (2011) *Biophys. J.* **101**, 386-395.

S3 Visscher, K. , Schnitzer, M. J. , and Block, S. M. (1999) *Nature* **400**, 184-189.